CBPF-NF-016/95

The Magnetic Properties of HoNiBC: Absence of Superconductivity and Helical Ground-State.

M. El Massalami, E. Baggio-Saitovitch and *A. Sulpice**

Centro Brasileiro de Pesquisas Físicas - CBPF
Rua Dr. Xavier Sigaud, 150
22290-180 – Rio de Janeiro, RJ – Brazil

*CNRS, CRTBT, BP166, 38042 Grenoble, Cedex 9 France

Abstract

The magnetic and transport properties of the quaternary intermetallic HoNiBC compound (space group P4/nmm, a = 3.563(1) $\mathring{A}$, c = 7.546(1)$\mathring{A}$) were studied for 1.2K$\leq$T$\leq$300K and H$\leq$80 kOe. The compound orders antiferromagnetically at 9.8(3)K and, in the ordered state, the Ho-moment saturates to 8.5(1)μ_B . In contrast with the structurally-related reentrant superconductor $HoNi_2B_2C$, neither superconductivity is found nor are there indications for a helical ground-state in the whole temperature range. These features are attributed, respectively, to the positioning of the Fermi level at a DOS minimum and the presence of the HoC double layers that inhibits the establishment of a helical spin arrangement.

Key-words: Intermetallic boro-carbide, HoNiBC, Antiferromagnetism.

1 Introduction

Recently two families of the nickel boro-carbide series $(RC)_n(Ni_2B_2)$ were discovered [1, 2]. The crystal structure of the much studied RNi_2B_2C family (n=1) is a filled variant on the $ThCr_2Si_2$-structure [3, 4]. It is a body-centered tetragonal structure (space group I4/mmm) where RC layers are alternately stacked on the Ni_2B_2 layers in the following sequences $(RC\text{-}B\text{-}Ni_2\text{-}B)_m$ (Fig.1.a). On the other hand, the structure of LuNiBC, as a representative of the less studied RNiBC family (n=2), adopts a simple tetragonal structure (space group P4/nmm) [3, 4]. In contrast with the layer stacking in the RNi_2B_2C family, the RC sheets are paired as double NaCl-type layers that are spatially separated by the Ni_2B_2 blocks resulting in the sequences $(RC\text{-}RC\text{-}B\text{-}Ni_2\text{-}B)_m$ (Fig.1.b).

It is interesting to see whether the above mentioned structural-chemical similarities of the two families are translated into similarity of the physical properties. On the one hand, the only studied member of the RNiBC series is LuNiBC [3, 4]. It is a metallic nonsuperconductor where the absence of superconductivity is shown, by electronic structure calculation to be due to the positioning of the Fermi level at a density of state (DOS) minimum [5]. On the other hand, the magnetic and the superconducting properties of the RNi_2B_2C family show quite interesting features[2,6-16]. As an example, the competition between superconductivity and magnetism in the R= Tm, Er, Ho, Dy, Tb, Gd compounds classify the series into the following different groups: superconducting antiferromagnets (R=Tm, Er, Ho (T<4K)), reentrant superconductor (Ho (4<T<5K) and normal-antiferromagnets (R=Dy, Tb, Gd). In particular, the origin of the reentrant behavior in $HoNi_2B_2C$ [7, 9, 10, 12, 13, 14] is related to the presence of the helical ground-state.

Our aim in this work is to study the magnetic and transport features of HoNiBC and to compare these properties with those of $HoNi_2B_2C$. In Sec.3, after asserting its structural character, we show that it is a nonsuperconducting AFM metal. In Sec.4, we associate the absence of the superconductivity and the helical ground-state in HoNiBC to its specific structural-chemical character.

2 Experimental

A conventional argon arc-melt method was used for sample preparation [2]. The as-prepared sample was wrapped in Ta-foil and vacuum-annealed for two days at 900C. After annealing, the button was quenched in liquid nitrogen. Standard powder Cu-Kα X-ray diffraction at ambient temperatures together with the Rietveld refinement analysis were used for structural characterization. The magnetization was measured on a commercial SQUID magnetometer. The ac susceptometer was driven by a 1 Oe sinusoidal field oscillating at 500Hz. The dc resistivity was measured in a four point geometry. The longitudinal magnetoresistivity ($j//H$) was measured in fields up to 80 kOe using the four-point dc resistivity method. The sample temperature was monitored by carbon glass

thermometer with its long axis set perpendicular to the field direction. Temperatures were corrected for magnetic field influence following the procedure described in Ref.[17]

3 Results

For the structural analysis of X-ray diffractogram (Fig.2), we assumed the same structural model which was proposed for LuNiBC [3, 4]: a tetragonal system with a space group P4/nmm. In fact, the atomic position, occupation and thermal parameters of LuNiBC [3, 4] were taken as the starting parameters for our Rietveld refinement procedures. The numerical convergence of the profile fit was limited only by the presence of unidentified impurity phases (the most strong lines are denoted by short vertical arrows in Fig.2). The results of the refinement are shown in Fig.2. The presence of considerable preferred orientation features is attributed to the misrepresentative aspect within the powdered sample resulting from preferred cleavage along the basal plane.

In Refs.3-4, it was shown that the width of the B-Ni_2-B layers (and thus the separating distance between the RC sheets) as well as most of the chemical bonding lengths in both of LuNiBC and $LuNi_2B_2C$ are almost equal. We found the same results when comparing the structural features of HoNiBC and $HoNi_2B_2C$.

Magnetic susceptibility measurements (Fig.3) show a Curie-Weiss (CW) behavior down to approximately 17K. The effective moment is found to be $11.3(1)\mu_B$ which is 9% higher than the theoretically expected value for Ho^{3+} ion ($10.4\mu_B$). In addition, Fig.3 shows that the paramagnetic characteristic temperature (θ) is 9.6(1)K while the long range antiferromagnetic (AFM) order sets-in at $T_N = 9.8(3)$K. Such a closeness between T_N and θ ($\frac{T_N}{\theta} = 1.02$) reflects a stronger three-dimensional magnetic character as compared to the one observed in $HoNi_2B_2C$ ($\frac{T_N}{\theta} = 3.85$) [6, 9]. Moreover, the Néel temperature for HoNiBC is almost twice that of $HoNi_2B_2C$ (Tab.1). Naturally, these features are connected with the increased number of the magnetic layers in the former compound. Fig.3 shows, in addition, two features that deserve some comments. First for $T < T_N$ considerable differences exist between Field-Cooled and Zero-Field Cooled measurements (see the inset of Fig.3). This effect may be attributed to the presence of a small amount (few %) of atomic disorder (such as C-deficiency or B-C site interchange) that are beyond XRD diffraction resolution. Secondly, the deviation from the CW-law starts well above T_N. This is most likely due to short range ordering. As obvious, Fig.3 shows the absence of superconductivity in the whole measured temperature range.

Magnetization isotherm at T=2K (Fig.4) shows a smooth monotonic rise with the applied field up to 30 kOe above which it shows a quasi-linear slow rise. The extrapolated saturation moment per Ho-ion is $8.5(1)\mu_B$. This value is 15% lower than the expected moment for ionic Ho^{3+} and 6% lower than the corresponding saturation moment of $HoNi_2B_2C$ [9] (see Tab.1). Since the 4mm point symmetry at the Ho-site in HoNiBC is lower than the 4/mmm at the corresponding site in $HoNi_2B_2C$, it is tempting then to attribute this lowering of the saturation moment to the influence of a stronger crystalline electric field.

No attempts were made to analyze the results of Fig.4 for spin-flop field or anisotropic forces because of the polycrystalline form of the sample. For comparison sake, we included the powder magnetization isotherm of $HoNi_2B_2C$ [14] as an inset in Fig.4. It is evident

that the moment saturation in HoNiBC is harder to achieve than in $HoNi_2B_2C$ indicating a stronger anisotropic forces. Furthermore, the inset of Fig.4 shows that on saturating the magnetic moment of the polycrystalline $HoNi_2B_2C$ and ramping down the field, the helical spin structure is revealed as step-like structure in the M-H curve [9, 14]. Therefore, the absence of any step-like structure in the magnetization isotherms of HoNiBC (Fig.4) and the smooth behavior of the susceptibility below T_N (see the inset in Fig.3) suggest that there is no helical spin arrangement in this compound.

DC resistivity (Fig.5) shows a conventional metallic behavior at high temperatures and, as evident, there are no traces of superconductivity down to 1.2K. The longitudinal magnetoresistivity ($j//H$) is shown in the inset of Fig.5. $\Delta\rho(H)/\rho(H=0)= [\rho(H)-\rho(H=0)]/\rho(H=0))$ shows that the magnetic contribution to the resistivity decreases monotonically with H. Mean Field Approximation relates $\Delta\rho(H)/\rho(H=0)$ to the thermally averaged Ho moment $< gJ >$along the field direction by the following relation[18]:

$$\Delta\rho(H)/\rho(H=0)\alpha < gJ >^2 \qquad (1)$$

It is expected that the $< gJ >$*versus* H curve at T=2K (Fig.4) to be similar to the curve at T=4.2K. Then, the experimentally determined $< gJ >$ in Fig.4 can be substituted into Eq.1 and can be compared to the measured $\Delta\rho(H)/\rho(H=0)$. This is shown in the inset of Fig.5 wherein the solid line is the scaling of $< gJ >^2$ to $\Delta\rho(H)/\rho(H=0)$ values. It may be worthy to recall that, first, the sample is a textured polycrystal and is contaminated with a minority impurity phases and secondly, no correction is made to subtract the contribution of the lattice and the temperature-independent resistivities. Nevertheless, it is assuring to find out that the inset of Fig.5 shows qualitative agreement with the prediction of Eq.1 in fields up to 60 kOe.

4 Discussion

It is shown in Sec.3 that although HoNiBC and $HoNi_2B_2C$ are structurally related, their physical behavior are distinctly different. Below we discuss two characteristic differences: the absence of superconductivity and helical spin arrangement.

Based on the structural isomorphism between LuNiBC and HoNiBC and assuming the validity of the rigid-band model[19], we expect their electronic band structures to be similar. Then, similar to the case of LuNiBC, the absence of superconductivity in HoNiBC indicates that the Fermi level is still at a DOS minimum. In other words, the replacement of the Lu-ion by the Ho-ion did not influence drastically the position of the Fermi level even though the substitutent has a larger ionic size and may contribute differently to the formation of the conduction band.

For the discussion of the magnetic properties, let us assume that the dominant RKKY-type interactions can be described as follows: ferromagnetic (FM) couplings within the planes and AFM couplings among the neighboring and next-neighboring planes. The observation that the sign of θ is positive forms an indication for dominant FM interactions (even though the AFM interactions are responsible for the long range 3-dimensional order). For instance, the in-plane FM interactions might be much stronger than the inter-planar AFM interactions.

From considerations of energy cost minimization, it is expected that the specific structural arrangement of the HoC layers will exclude, at T=0, the helical spin state in favor of the AFM arrangement as shown in Fig.1.b. A helical state will be expected only if the AFM-coupled layers are evenly spaced along the spiral axis[18]. This is the case of $HoNi_2B_2C$ [7, 13] wherein the AFM coupled HoC layers are evenly spaced along the c-axis and so makes it possible to sustain a constant spiral angle between the moment orientations of adjacent FM sheets.

5 Conclusion

The insertion of additional HoC layers in the structure of $HoNi_2B_2C$ leads to drastic changes in the physical properties of the resulting HoNiBC compound. The Fermi level is shifted to a DOS minimum (thus no superconductivity). The average strength of the magnetic couplings is enhanced as reflected in higher values of the ordering temperature and the saturation field. Furthermore, the resulting uneven spacing of the HoC layers seems to destabilize the helical state in favor of a simple AFM state.

Acknowledgement

R.Pereira is thanked for taking the XRD diffractogram.

Table Captions

Tab.1 Comparison of some of the structural and magnetic properties of HoNiBC and $HoNi_2B_2C$. The magnetic data of $HoNi_2B_2C$ are taken from Refs.[6, 9].

compound	space group	Ho-site symmetry	a ($\mathring{A}$)	c ($\mathring{A}$)	μ μ_B	T_N (K)	θ (K)
HoNiBC	P4/nmm	4mm	3.563(1)	7.546(1)	8.5(1)	9.8(3)	9.6(1)
$HoNi_2B_2C$	I4/mmm	4/mmm	3.520(1)	10.521(1)	9.0	5.0	1.3

Figure Captions

Fig.1. The ac-plane projection of the structural features and the magnetic ground state at T=0 K of $HoNi_2B_2C$ and HoNiBC. The units cells are marked by dotted lines. The arrows indicate the orientations of the Ho-moments.

Fig.2. The Cu-Kα diffractogram of HoNiBC. The mid field shows the experimental points (dots) and the theoretical fit (continuous line). The Bragg lines are shown at the top field (short vertical bar) while the difference (continuous line) is shown in the lower field. The most strong peaks of the impurity phases are denoted by two short vertical arrows. The text-inset gives some of the obtained structural parameters.

Fig.3. Field-Cooled (FC) and Zero-Field-Cooled (ZFC) magnetic susceptibilities of HoNiBC. The inset shows the ac susceptibility at zero field (stars) as well as the FC (filled circles and triangles) and ZFC (empty circles and triangles) dc susceptibilities at different fields.

Fig.4. The magnetization isotherm at T=2K of HoNiBC. The inset shows the magnetization isotherm for $HoNi_2B_2C$ at 1.7K wherein the two intermediate field-induced phase transitions are denoted by vertical arrows [14].

Fig.5. The dc resistivity in zero-field of HoNiBC. *The inset:* The longitudinal ($j//H$) magnetoresistivity is shown as $[\rho(H) - \rho(H = 0)]/\rho(H = 0)$ *versus* H without subtracting the nonmagnetic contribution to the resistivity. The solid line in the insert shows the scaling to $< gJ >^2$(see text).

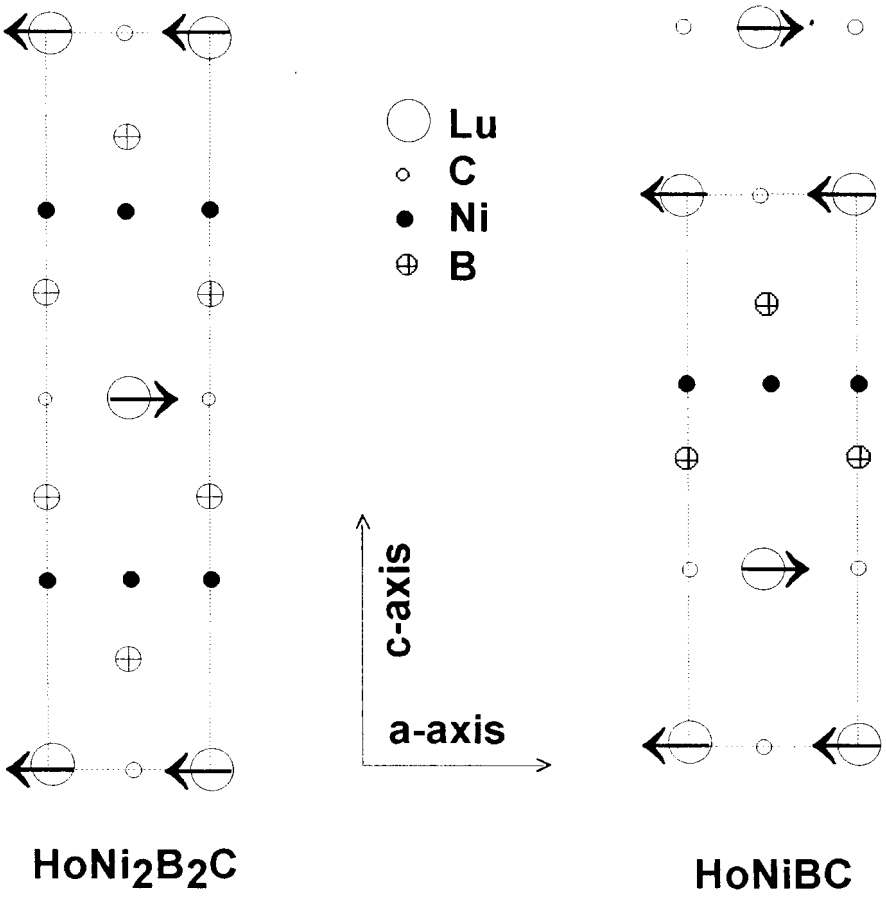

Fig.1

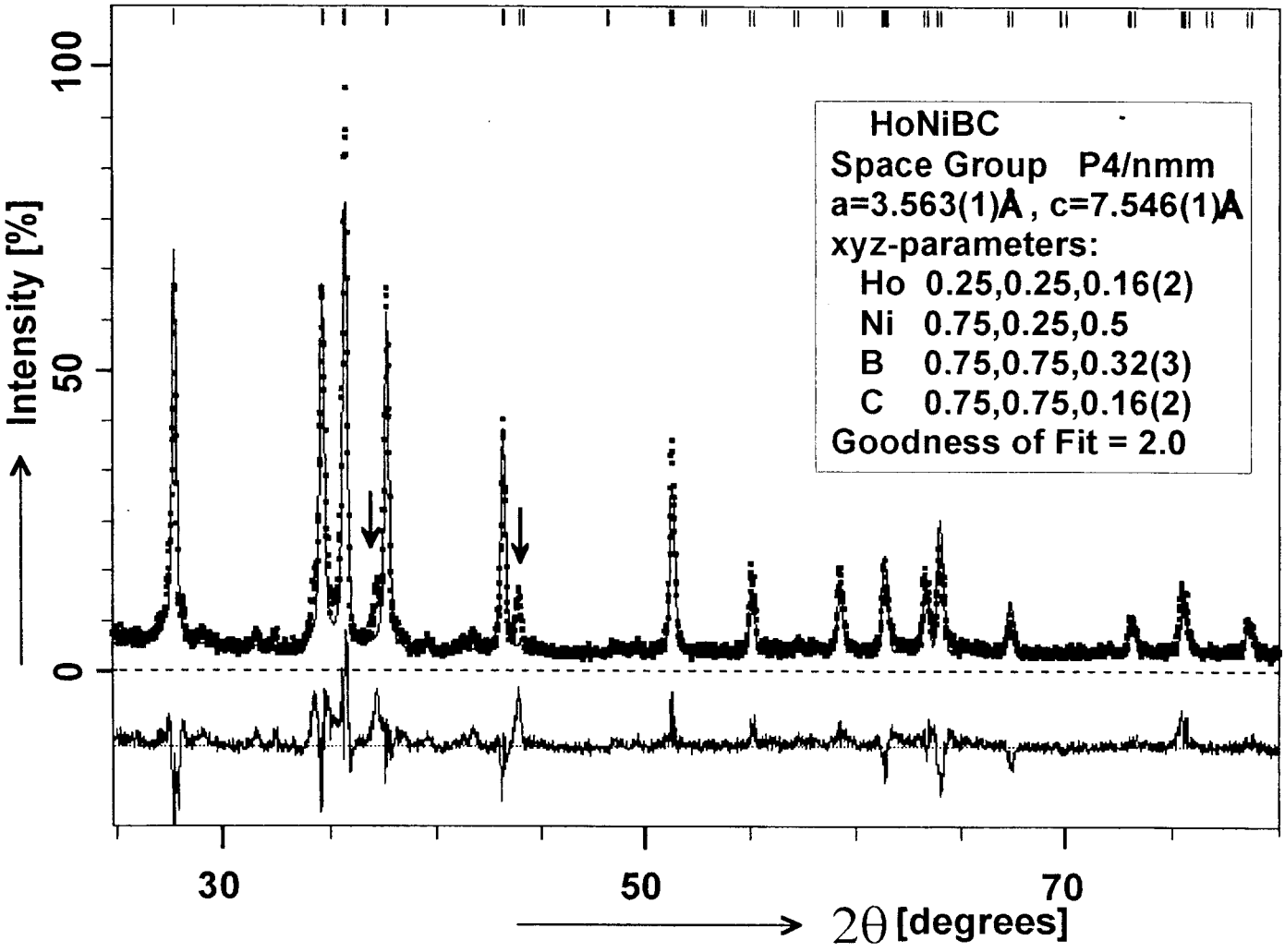
HoNiBC
Space Group P4/nmm
a=3.563(1)Å , c=7.546(1)Å
xyz-parameters:
Ho 0.25,0.25,0.16(2)
Ni 0.75,0.25,0.5
B 0.75,0.75,0.32(3)
C 0.75,0.75,0.16(2)
Goodness of Fit = 2.0
Intensity [%]
100
50
0
30
50
70
2θ [degrees]

Fig.2

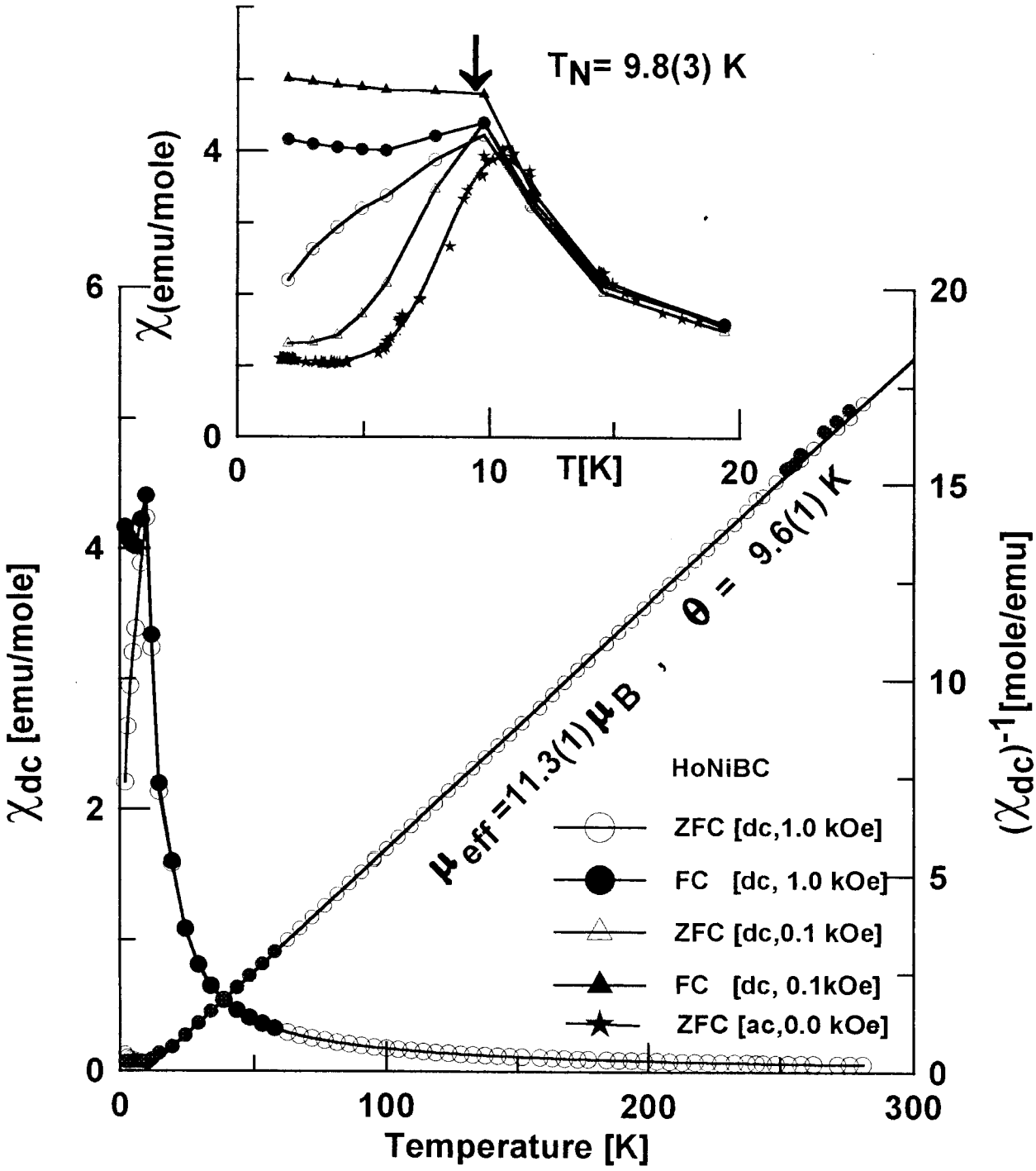
T_N= 9.8(3) K
χ(emu/mole)
T[K]
χdc [emu/mole]
(χdc)-1[mole/emu]
Temperature [K]
μeff =11.3(1)μB , θ = 9.6(1) K
HoNiBC
ZFC [dc,1.0 kOe]
FC [dc, 1.0 kOe]
ZFC [dc,0.1 kOe]
FC [dc, 0.1kOe]
ZFC [ac,0.0 kOe]

Fig.3

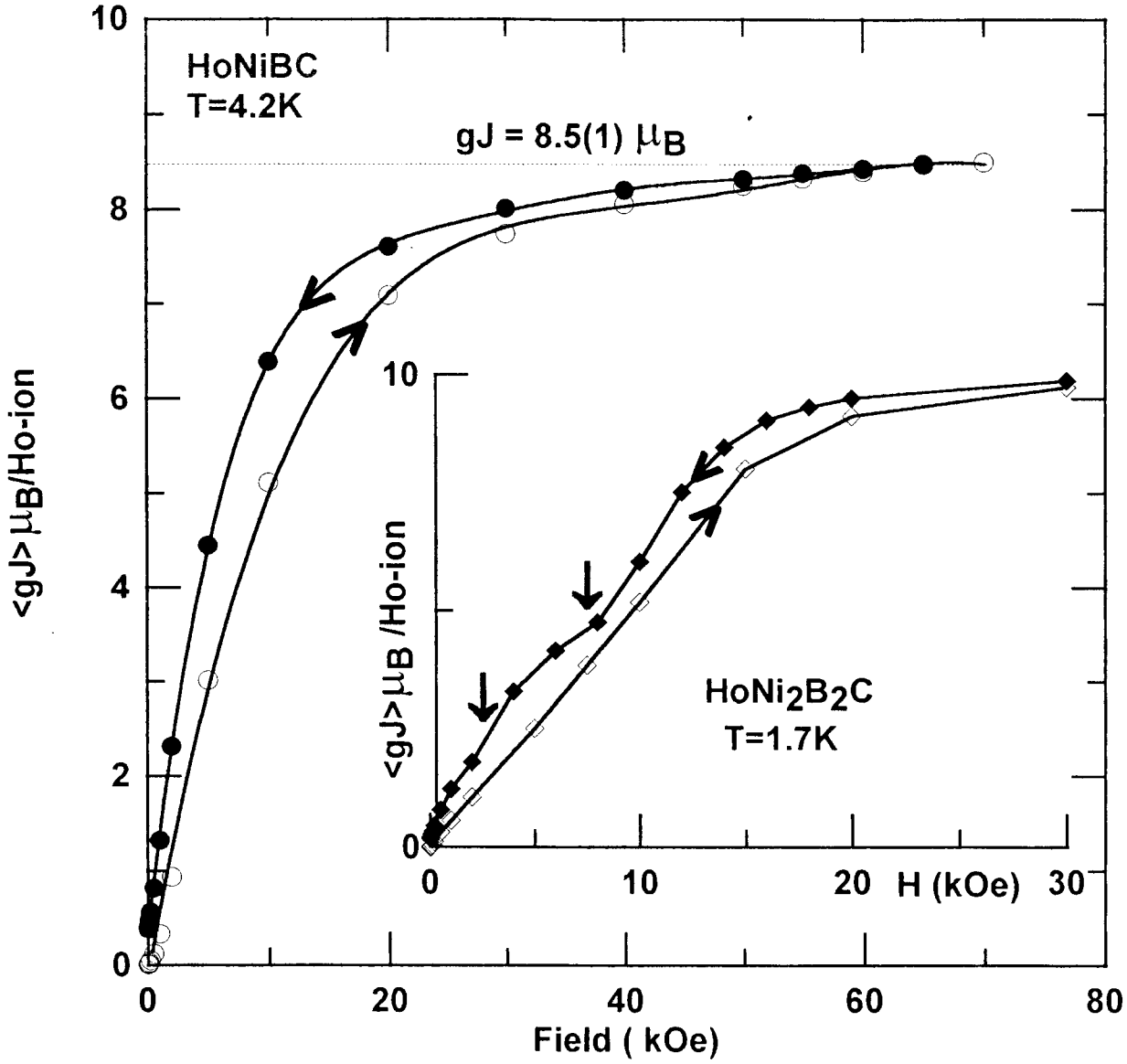
HoNiBC
T=4.2K
gJ = 8.5(1) μB
<gJ> μB/Ho-ion
Field (kOe)
HoNi2B2C
T=1.7K
<gJ> μB /Ho-ion
H (kOe)

Fig.4

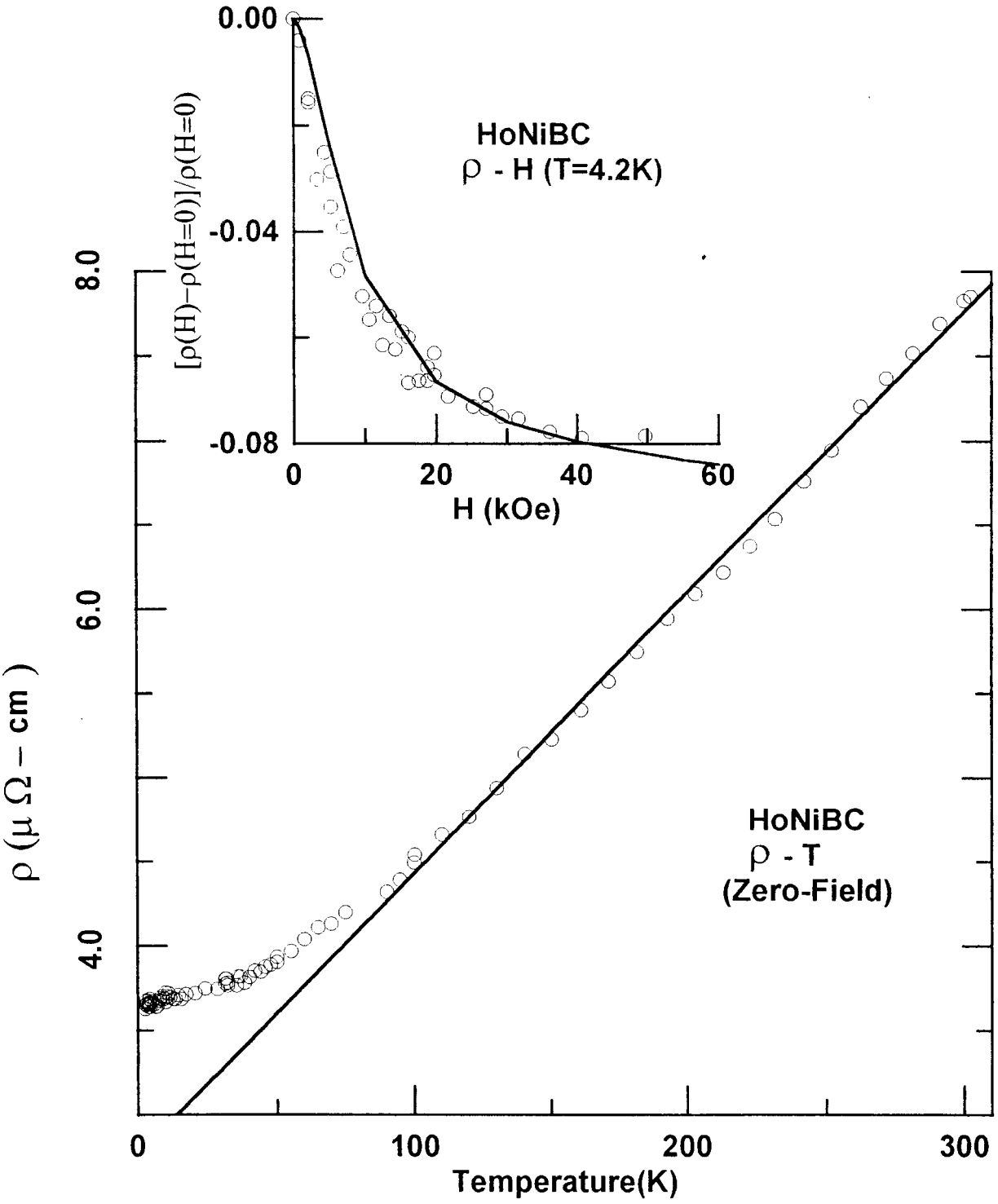
HoNiBC
ρ - H (T=4.2K)
[ρ(H)–ρ(H=0)]/ρ(H=0)
0.00
-0.04
-0.08
0
20
40
60
H (kOe)
HoNiBC
ρ - T
(Zero-Field)
ρ (μ Ω – cm)
8.0
6.0
4.0
0
100
200
300
Temperature(K)

Fig.5

References

[1] R. Nagarajan, C. Mazumdar, Z. Hossein, S.K. Dhar, K.V. Golpakrishna, L.C. Gupta, C. Godart, B.D. Padalia and R. Vijayaragharan, Phys.Rev.Lett. 72(1994)274.

[2] R.J. Cava, H. Takagi, B. Batlogg, H.W. Zandbergrn, J.J. Krajewski, W. F. Peck, Jr, T. Siegrist, B. Batlog, R. B. van Dover, R. J. Felder, K. Mizuhashi, J.O. Lee, H. Eisaki, and S. Uchida, Nature 367(1994)252.

[3] T. Siegrist, H.W. Zandbergen, R.J. Cava, J.J. Krajewski and W. F.Peck, Nature 367 (1994) 252.

[4] H.W. Zandbergen, R.J. Cava, J.J. Krajewski, W.F. Peck, Jr., Physica C224(1994)6.

[5] L.F. Mattheiss, Phys.Rev. B49(1994) 13279.

[6] H. Eisaki, T. Takagi, R.C. Cava, K. Mizuhashi, J.O. Lee, B. Batlogg, J.J. Krajewski, W.F. Peck and S. Uchida, Phys.Rev.B 50(1994)647.

[7] T.E. Grigereit, J.W. Lynn, Q. Huang, A. Santoro, R.J. Cava, J.J. Krajewski and W.F. Peck, Jr, Phys.Rev. Let. 73(1994)2756; Q. Huang, A. Santoro, T.E. Grigereit, J.W.Lynn, R.C. Cava, J.J. Krajewski and W.F. Peck, Phys. Rev.B51(1995, in press).

[8] R. Movshovich, M.F. Hundley, J.D. Thompson, P.C. Canfield, B.K. Cho, A.V. Chubukov, Physica C 227(1994)381.

[9] P. C. Canfield, B. K Cho, D. C. Johnston, D. K. Finemore, M. F. Hundley, Physica C 230 (1994) 397.

[10] M.El Massalami, S.L. Bud'ko, B. Giordanengo and E.M. Baggio-Saitovitch, Physica C in press.

[11] S.K. Sinha, J.W. Lynn, T.E.Griegereit, Z. Hossain, L.C. Gupta, R. Nagarajan and C.Godart, Phys.Rev.B51(1995, in press).

[12] H. Schmidt and H.F. Braun, Physica C 229(1994)315.

[13] A. I. Goldman, C. Stassis, P. C. Canfield, J. Zarestky, P. Dervenagas, B. K.Cho and D. C. Johnston, Phys.Rev.B 50(1995)9668.

[14] M.El Massalami et al, preprint.

[15] M. El Massalami, S. L. Bud'ko, B. Giordanengo, M. B. Fontes, J. C. Mondragon and E.M. Baggio-Saitovitch, PhysicaC 235-240(1994)2563, M.El Massalami, S.L. Bud'ko, B. Giordanengo, M.B. Fontes, J.C. Mondragon and E.M. Baggio-Saitovitch, Physica Status Solidi (b) in press.

[16] B. Giordanengo, M. El Massalami, S.L. Bud'ko, E.M. Baggio-Saitovitch, J.Voirn and A. Sulpice, preprint.

[17] H.H. Sample, B.L. Brandt and L. G. Rubin, Rev. Sci. Instrum. 53(1982)1129.

[18] B. Coqblin , The Electronic Structure of Rare-Earth Metal and Alloys: the Magnetic Heavy Rare-Earth (Academic Press, London, 1977).

[19] S.V. Vonsovsky, Yu.A. Izyumov and E.Z. Kurmaev; Superconducitivity of Transition Metals (Springer series in Solid-state Sciences 27,N.Y., 1982).